Journal of Materials Chemistry A

PAPER

View Article Online
View Journal | View Issue

Cite this: J. Mater. Chem. A, 2014, 2, 19556

Dye sensitized solar cells with cobalt and iodine-based electrolyte: the role of thiocyanate-free ruthenium sensitizers†

Kuan-Lin Wu,‡[a] Yue Hu,‡[b] Chun-Tien Chao,[a] Ya-Wen Yang,[a] Ting-Yun Hsiao,[c] Neil Robertson*[b] and Yun Chi*[a]

Received 14th August 2014
Accepted 7th October 2014

DOI: 10.1039/c4ta04208e

www.rsc.org/MaterialsA

Three isomeric Ru(II) metal complexes with distinctively oriented tpiq ancillary chelates, **TFRS-80a**, **80b** and **80c**, were prepared from the condensation of Ru(4,4′-diethoxycarbonyl-2,2′-bipyridine) (*p*-cymene)Cl with tpiqH, *i.e.* 6-(5-(2,6-bis(hexyloxy)phenyl)thiophen-2-yl)-1-(3-(trifluoromethyl)-1*H*-pyrazol-5-yl)-isoquinoline. Photophysical and electrochemical investigations, together with DFT and TD-DFT calculations, allowed a comprehensive understanding of their basic properties in both solution state and on TiO_2 surface. DSC cells with both an ultra-thin layer of transparent TiO_2 (3.6 μm) and I^-/I_3^- electrolyte were fabricated, for which the symmetric sensitizers **TFRS-80a** and **80c** showed better performances (η = 8.37 and 8.26%) over that of the asymmetric counterpart **TFRS-80b** (η = 5.55%), the latter suffered from poor dye loading and consequently lowered J_{SC} and V_{OC}. In sharp contrast, all DSC cells with $[Co(phen)_3]^{2+/3+}$ electrolyte gave superior efficiencies (η = 8.36–9.06%), for which the thiocyanate-free architecture, the improved light harvesting capability, and the possession of conjugated and bulky 5-(2,6-bis(hexyloxy)phenyl)thiophen-2-yl functional moieties are three primary factors governing the observed results.

Introduction

Photovoltaic technologies are pivotal to the future progression of human societies, among which dye-sensitized solar cells (DSCs)[1] have already achieved a highest conversion efficiency of ~13%, using Zn(II) porphyrin sensitizers together with $Co^{2+/3+}$ electrolytes.[2] A typical DSC consists of a dye that self-assembles onto a mesoporous TiO_2 photoanode. The sensitizers can rapidly inject electrons into the conduction band of the TiO_2, following excitation by incident solar irradiation. The oxidized sensitizers are then regenerated by redox couples in the electrolyte and become available for the next round of light harvesting, electron injection and reduction. It is believed that better sensitizers would offer a leap in improvement in the overall efficiency of DSC devices.

Organic donor–acceptor dyes with cyanoacrylic anchor are highly competitive due to their potentially simple design, synthetic flexibility and scalability.[3] However, their disadvantage is the poor stability under the combined effects of UV irradiation and water content in the electrolyte, which triggers both the reversion of cyanoacrylic acid to aldehyde,[4] and photoisomerization of acrylic C=C bond.[5] Recently, a class of organic dyes bearing benzoic acid have ingeniously avoided these degradation pathways and, in combination with filling defects on the TiO_2 surface to attenuate interfacial charge recombination, showed excellent efficiency of >12% with $Co^{2+/3+}$ electrolytes.[6]

Ru(II) complexes with thiocyanate ancillaries are known to be both efficient and relatively stable;[7] hence, they have been subjected to advanced studies aimed towards possible commercialization.[8] On the other hand, there are growing studies on Ru(II) sensitizers devoid of thiocyanate ligand, among which van Koten and coworkers have utilized cyclometalate ancillaries to construct the first class of thiocyanate-free Ru(II) sensitizers, albeit of lower efficiency.[9] However, their true potential was only realized after Grätzel, who employed the electron deficient 2,4-difluorophenyl pyridinato chelate to construct the sensitizer YE05, showed a prominent conversion efficiency (η) of 10.1% at standard AM 1.5 sunlight.[10] Later, cyclometalates and other ancillaries were systematically employed by Berlinguette in attempts to expand this class of Ru(II) sensitizers.[11]

In this content, our group has carried out studies using N-donor ancillaries, such as pyridyl azolate,[12] 2,6-diazolyl

[a]Department of Chemistry and Low Carbon Energy Research Center, National Tsing Hua University, Hsinchu 30013, Taiwan. E-mail: ychi@mx.nthu.edu.tw

[b]EaStCHEM, School of Chemistry, University of Edinburgh, King's Buildings, West Mains Road, Edinburgh EH9 3 JJ, UK. E-mail: Neil.Robertson@ed.ac.uk

[c]Department of Engineering and System Science, National Tsing Hua University, Hsinchu 30013, Taiwan

† Electronic supplementary information (ESI) available. See DOI: 10.1039/c4ta04208e

‡ K.-L. W. and Y. H. contributed equally to this work.

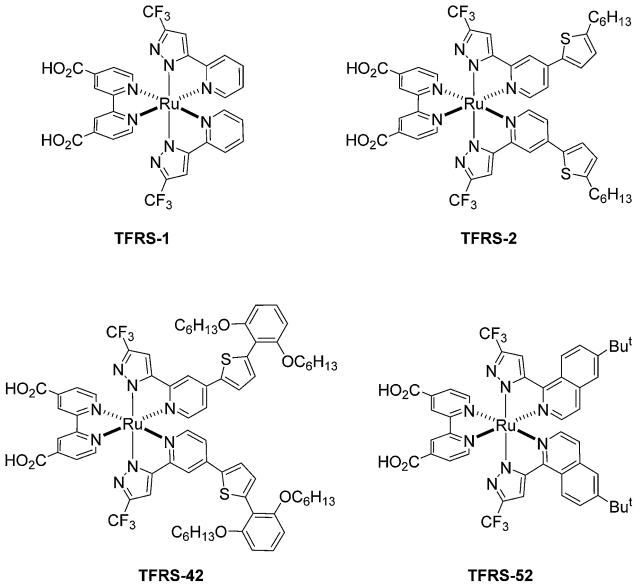

Scheme 1 Structures of sensitizers TFRS-1, 2, 42 and 52.

pyridine[13] and 2-azolyl-6-phenylpyridine,[14] to replace the aforementioned cyclometalates. Scheme 1 depicts three Ru(II) sensitizers with *trans*-substituted pyrazolate fragments, all derived from their parent complex **TFRS-1**, showing respectable η of ≥10% using I^-/I_3^- based electrolyte for **TFRS-52**,[15] and η of 8.71% using $[Co(bpy)_3]^{2+/3+}$ electrolyte for **TFRS-42**, respectively.[16] It is notable that **TFRS-42** exhibited the highest η for the $Co^{2+/3+}$ electrolytic system due to its charge neutrality, greater spatial congestion and absence of thiocyanate ligands, all of which are essential for reducing the recombination across the interface of TiO_2 and electrolyte.

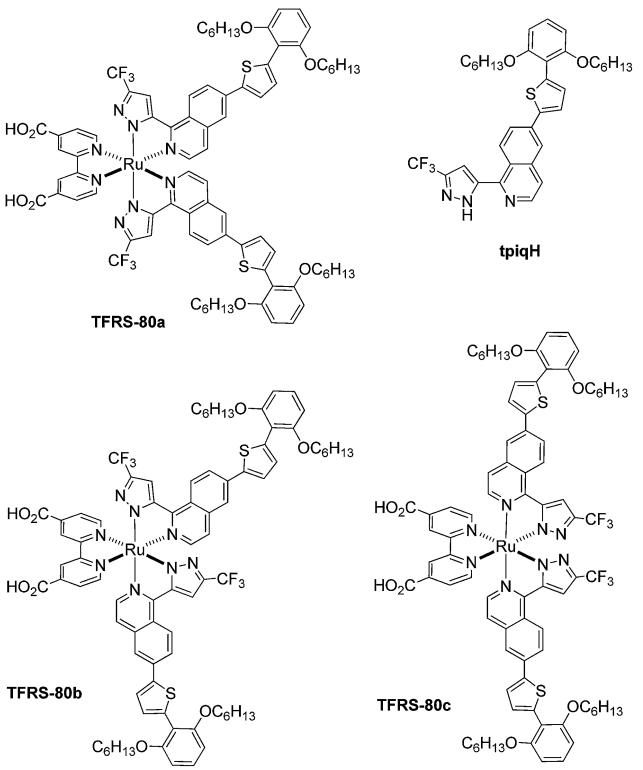

Scheme 2 Structural drawings of tpiqH chelate and isomeric sensitizers TFRS-80a, 80b and 80c.

These TFRS sensitizers were prepared by coupling of Ru(diethyl 2,2′-bipyridine-4,4′-dicarboxylate) (*p*-cymene)Cl with two equiv. of chelating pyrazole, followed by hydrolysis in basic media. In the absence of any regioselectivity, a maximum of three isomers would be expected, for which the other two structures would differ from all the *trans*-substituted TFRS dyes shown in Scheme 1 by reshuffling the orientation of the azolate chelates.[17] Herein, we wish to report the detailed study on the system where all three isomeric sensitizers, **TFRS-80a**, **80b** and **80c**, have been isolated and characterized. These sensitizers are derived from a π-conjugated tpiqH chelate, *i.e.* 6-(5-(2,6-bis-(hexyloxy)phenyl)thiophen-2-yl)-1-(3-(trifluoromethyl)-1*H*-pyrazol-5-yl)isoquinoline, such that their higher absorptivity and potential for fabrication of DSCs with high η of 9.06% triggered the full determination of their photophysical and electrochemical properties and structure-efficiency relationship of both I^-/I_3^- and $Co^{2+/3+}$ based dye-sensitized solar cells (Scheme 2).

Results and discussion

Syntheses

The pyrazolate ancillary, 5-(2,6-bis(hexyloxy)phenyl)thiophen-2-yl substituted tpiqH chelate, was selected for this investigation due to the large π-conjugation expected for both the isoquinolinyl fragment and thienyl appendage at the C6 position, resulting in a combined hyperchromic effect and bathochromic shift in the recorded UV/Vis spectra. Moreover, the main function of the 2,6-dihexyloxylphenyl group is to provide both further increased π-conjugation on the whole molecule and tailored steric encumbrance over the thienyl fragment, such that the formation of intermolecular π–π-stacking interactions around the isoquinolinyl entities can be effectively suppressed. This knowledge is obtained from the molecular design of several efficient DSC sensitizers, on which similar 2,6-dialkoxyphenyl groups were incorporated for suppressing aggregation, improving the solubility in organic solvents, and enhancing the overall efficiency of the fabricated DSC devices.[18]

This chelating ancillary is treated with the metal reagent Ru(4,4′-diethoxycarbonyl-2,2′-bipyridine) (*p*-cymene)Cl and the basic promoter KOAc in xylenes, according to the established protocol. All three isomeric products were separated using SiO_2 column chromatography, after executing two consecutive elutions using a 1 : 4 mixture of ethyl acetate and hexane, followed by employment of a 1 : 20 mixture of ethyl acetate and CH_2Cl_2. Subsequent hydrolysis of each compound in NaOH–water–acetone mixture afford the carboxylic sensitizers **TFRS-80a**, **80b** and **80c** in 32%, 11% and 15% yields, respectively. It is notable that these isomers represent formation of all three possible structural isomeric Ru(II) based complexes, for which their structural identification can be achieved according to their ^1H and ^{19}F NMR spectral pattern. Of particular

importance is the ^{19}F NMR spectral data, which unambiguous confirmed the symmetric or asymmetric nature of **TFRS-80a**/**80c** and **TFRS-80b** by revealing a single ^{19}F NMR signal and two signals of equal intensity, respectively.

Photophysical and electrochemical behavior

The absorption spectra of **TFRS-80a**, **80b** and **80c** were measured in DMF and are depicted in Fig. 1, while pertinent numerical data are summarized in Table 1. As can be seen, all sensitizers show strong absorption at ~360 nm with extinction coefficient (ε) falling in the range of 5.1–6.2 $\times$ 10^4 M^{-1} cm^{-1}, which is apparently due to the ligand centered π–π^* transition. In addition, there is another lower energy, broad transition centered at ~525 nm, with a slightly lower extinction coefficient of 3.2–3.9 $\times$ 10^4 M^{-1} cm^{-1}. Furthermore, the recorded extinction coefficients are all markedly higher than the corresponding band of **N719** (1.4 $\times$ 10^4 M^{-1} cm^{-1}) and relevant MLCT band of **C101** (1.75 $\times$ 10^4 M^{-1} cm^{-1})[19] and **TG6** (2.3 $\times$ 10^4 M^{-1} cm^{-1}),[20] confirming the excellent light harvesting capability in the visible region. The comparisons of experimental UV-visible spectra with the computational simulated oscillator strengths are presented in Fig. S1–S3 of ESI.†

DFT and TD-DFT calculations using a DMF polarizable continuum model were carried out, showing that in each case the LUMO is based upon the dicarboxy bipyridine as expected, and that the HOMO is distributed across the Ru orbitals and the entire tpiq ligand (Fig. 2). In particular, we note that this conjugation extends to the thienyl and 2,6-dihexyloxylphenyl fragments in keeping with the intended ligand design and ensuring effective charge separation between electrons injected into the TiO_2 and the positive charge on the oxidized dye. It is also apparent that the delocalization of the HOMO differs across the isomer series, with only that of **TFRS-80a** spread across both tpiq ligands, presumably accounting for the lower HOMO energy for this dye. The TD-DFT calculations reproduced the transition energies of the charge-transfer bands moderately well, with the results sufficient to give insight into the orbital origins of transitions. The 525 nm charge transfer band in each case (calculated at around 480 nm) originates from a mixture of the Ru(II) metal core and the pyrazolate to dicarboxy bipyridine, *i.e.* a mixing of MLCT and LLCT transitions, in a way analogous to the assignment made for other TFRS sensitizers.[12b]

In the context of DSC application, further enhancements in absorption were observed upon depositing these sensitizers on the TiO_2 surface, such that all of the absorptions broadened substantially, the recorded spectra showed an absence of the semi-transparent region centered at 430 nm recorded in DMF solution, as well as red-shifting of the lowest energy absorption peak maxima to ~700 nm. We speculate that such a broadened spectral profile is beneficial to the competitive harvesting of shorter wavelength irradiation,[21] particular for DSC devices that utilize the I^-/I_3^- based electrolytes.

Table 1 Photophysical and electrochemical data of the studied sensitizers recorded in DMF at RT

Dye	λ_{abs} [nm] (ε $\times$ 10^{-3} [M^{-1} cm^{-1}])	$E^{\circ\prime a}_{ox}$	E_{0-0} [b]	$E^{\circ\prime *}$ [c]
TFRS-80a	309 (54), 360 (62), 523 (39)	0.87	1.89	−1.00
TFRS-80b	310 (51), 366 (64), 524 (37)	0.83	1.90	−1.07
TFRS-80c	308 (44), 362 (51), 527 (32)	0.78	1.87	−1.09

[a] Oxidation potential of dye was measured in DMF with 0.1 M [TBA][PF_6] and with a scan rate of 50 mV s^{-1}. It was calibrated with Fc/Fc^+ reference and converted to NHE by addition of 0.63 V. [b] E_{0-0} was determined from the intersection of the absorption and the tangent of emission peak in DMF. [c] $E^{\circ\prime *} = E^{\circ\prime}_{ox} - E_{0-0}$.

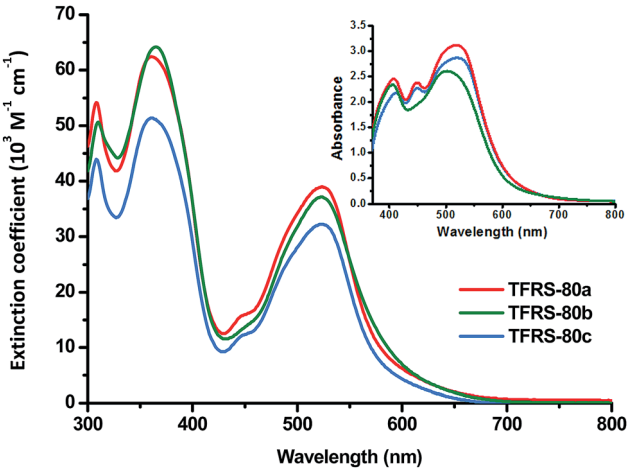

Fig. 1 UV/Vis absorption spectra of various TFRS-80 sensitizers (1 $\times$ 10^{-5} M) in DMF. Inset: spectra of samples adsorbed on 5 μm transparent TiO_2 thin film.

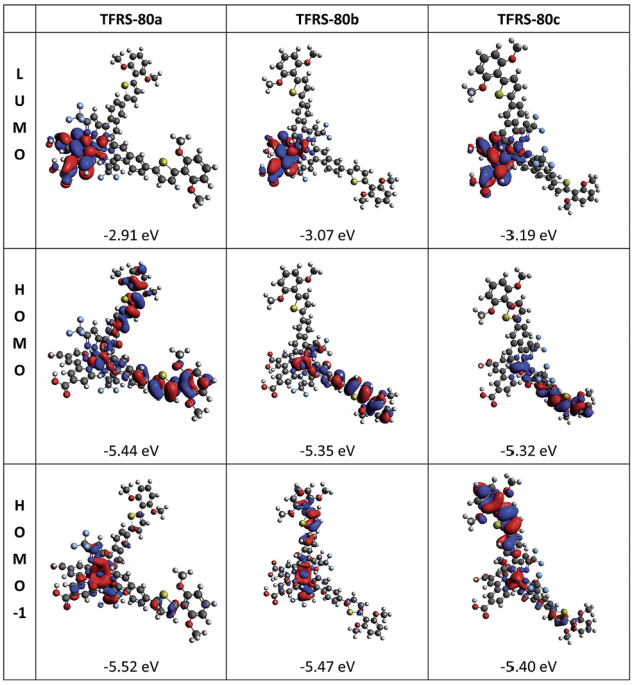

Fig. 2 Molecular orbital distributions and energy of Ru(II) sensitizers (isodensity = 0.020 a.u.).

Cyclic voltammetry was conducted to reveal the variation in electrochemical potentials among the three isomers, and to verify whether the oxidation potential of the ground state ($E^{\circ\prime}_{ox}$) matches the redox potential of the redox mediators. As shown in Table 1, the oxidation potential of the isomers follows the trend of **TFRS-80c** < **80b** < **80a** which are reproduced well by the calculated HOMO energies shown by the computational results (see Tables S1–S3†). The $E^{\circ\prime}_{ox}$ is attributed to the Ru(II) metal oxidation, and appeared in the range of 0.78–0.87 V (*vs.* NHE, normal hydrogen electrode), all more positive than that of I^-/I_3^- redox couple (E° = *ca.* 0.4 V) and the redox potential of the $[Co(phen)_3]^{2+/3+}$ (E° = *ca.* 0.62 V *vs.* NHE). The limited variation in $E^{\circ\prime}_{ox}$ potentials in these studies can be attributed to the identical local coordination environment around the central Ru(II) atom, with the small differences attributed to different amounts of delocalization and stabilization of the HOMO. In addition, the zero–zero transition energy (E_{0-0}) or band gap was determined from the intersection of the absorption and normalized emission spectra. From this, the excited-state oxidation potential ($E^{\circ\prime}$*) is estimated from the difference of $E^{\circ\prime}_{ox}$ and E_{0-0}, from which the calculated values of −1.00 to −1.09 V (*vs.* NHE) were obtained. Since all of the $E^{\circ\prime}$* are significantly more negative than the conduction band edge of the TiO_2 electrode ($E_{CB} \sim -0.2$ and −0.5 V *vs.* NHE),[22] this confirms that efficient electron injection from the excited sensitizer to the conduction band of TiO_2 should occur.

To probe the longer-term stability of the dye oxidized state we carried out spectroelectrochemical studies of each dye in solution upon oxidation (Fig. S4–S6†). It was apparent that **TFRS-80c** showed the best isosbestic points during the oxidation and was more fully returned to the starting spectrum upon reduction in comparison with either **TFRS-80a** or **TFRS-80b**. We have previously suggested the possibility of some isomerization within this type of dye series upon oxidation,[17] which may also provide an explanation in this case. We note however, that as for previous **TFRS-2** and **TFRS-52** dyes, the oxidative stability was much higher than we have observed for thiocyanate-containing dyes such as N3.[17]

To further clarify the influence of the dye structure on the solar cell performance (described in the next section), we carried out electrochemical studies of the dyes bound to mesoporous TiO_2 films. Since the electrochemical window used lies entirely within the band gap of the TiO_2, the TiO_2 remains insulating and the redox occurs *via* a hole-diffusion process starting from the base of the film where dye is in contact with the FTO electrode. Firstly, we observe excellent reversibility of the redox process for all three isomers (Fig. S7–S9†) with little change between redox cycles 1 to 51 confirming these as stable sensitizers. This observation is different from that of **TFRS-2** and **52**, for which the asymmetric isomer **b** is found to be more stable *versus* the respective isomer **a**.[17] Moreover, the quantity of dye uptake was observed to be **TFRS-80a** > **c** > **b**, (Table S4†) consistent with that observed during DSC fabrication (see below). Furthermore, following previously-described procedures and equations listed in ESI,† the maximum observed current and dye concentration were used to calculate a hole-diffusion coefficient for the case of each dye and these were observed to be in the order **TFRS-80a** > **80b** > **80c** (4.21, 1.28 and 0.203 × 10^{-10} cm^2 s^{-1} respectively). These values are all 1–3 orders of magnitude lower than typical values reported for other Ru and organic dyes.[23] It seems likely that this arises due to success of the design strategy whereby the 2,6-dihexyloxylphenyl on the tpiq ligand can suppress π–π interactions and avoid aggregation. In addition, the order of the values among the isomers further supports this conclusion, since **TFRS-80a**, **80b** and **80c** have respectively zero, one and two tpiq arms in the plane of the surface to minimize dye–dye electronic interactions.

Device characteristics

The photovoltaic properties of these sensitizers were examined, for which the details of cell fabrication and data measurements are depicted in the Experimental section. All cells were fabricated using 3.6 μm (20 nm) + 3.5 μm (400 nm) of mesoporous TiO_2 thin film. The photocurrent–voltage characteristics were summarized in Tables 2 and 3. Three electrolyte solutions were employed for these studies; the first (*i.e.* electrolyte I–A) consisted of 0.6 M 1,2-dimethyl-3-propylimidazolium iodide (DMPII), 0.05 M I_2, and 0.5 M *t*-butylpyridine (TBP) in acetonitrile, while the second (*i.e.* $Co(phen)_3]^{2+/3+}$ electrolyte Co-phen) and the third (*i.e.* electrolyte I–B) contained 0.45 M $[Co(phen)_3][TFSI]_2$, 0.15 M $[Co(phen)_3][TFSI]_3$, 0.15 M LiTFSI, 0.8 M TBP in acetonitrile, as well as 0.45 M DMPII, 0.05 M I_2, 0.15 M LiI, 0.8 M TBP in acetonitrile, respectively. The electrolyte I–A possesses no Li^+, while both Co-phen and I–B contain 0.15 M of Li^+ cation in electrolyte, such that they can provide an intimate comparison between cell characteristics of the cobalt and iodine based redox couples. Comparative studies on cells with both I^-/I_3^- and $Co^{2+/3+}$ electrolytes are starting to gain momentum, inspired by the recent report that the $Co^{2+/3+}$ cells have shown promising photostability under full sun solar illumination.[24]

For the DSCs using electrolyte I–A, **TFRS-80a** exhibited a J_{SC} of 12.93 mA cm^{-2}, a V_{OC} of 890 mV, and a fill factor (FF) of 0.727, while **TFRS-80c** gave performance data of 12.41 mA cm^{-2}, 880 mV and 0.756, respectively. Their overall conversion efficiencies (η) were calculated to be 8.37% and 8.26%, hence both are superior to that obtained for the asymmetric sensitizer **TFRS-80b**, with J_{SC} = 9.81 mA cm^{-2}, V_{OC} of 780 mV, FF = 0.725 and η = 5.55%. Since the mixture of isomers **80a** and **80c** can be easily

Table 2 Performance characteristics for DSCs based on I^-/I_3^- electrolyte I–A under AM 1.5G irradiation[a]

Dye	J_{SC} [mA cm^{-2}]	V_{OC} [mV]	FF	η [%]	Dye loading[b]
TFRS-80a	12.93	890	0.727	8.37	1.72
TFRS-80b	9.81	780	0.725	5.55	1.03
TFRS-80c	12.41	880	0.756	8.26	1.21
TFRS-80ac	13.12	870	0.731	8.34	

[a] All devices were fabricated using methods depicted in the Experimental section. [b] Dye desorption experiment was performed using 1 M TBAOH in water–MeOH (v/v, 1 : 1). The dye loading is in unit of 10^{-7} mol cm^{-2}.

Table 3 Performance characteristics for DSCs based on $Co^{2+/3+}$ electrolyte Co-phen and I^-/I_3^- electrolyte I–B, under AM 1.5 G irradiation

Dye	Electrolyte	J_{SC} [mA cm^{-2}]	V_{OC} [mV]	FF	η [%]
TFRS-80a	Co-phen	13.44	840	0.757	8.55
	I–B	14.49	780	0.668	7.55
TFRS-80b	Co-phen	13.30	820	0.766	8.36
	I–B	10.39	680	0.681	4.80
TFRS-80c	Co-phen	14.32	840	0.754	9.06
	I–B	14.84	730	0.651	7.06

separated from **80b**, but separation of **80a** and **80c** required repeated column chromatography, from the point view of practical application we therefore attempted DSC fabrication using the naturally occurring mixture of **TFRS-80a** and **80c**, for which the recorded characteristics were J_{SC} = 13.12 mA cm^{-2}, V_{OC} of 870 mV, FF = 0.731, and η = 8.34%, respectively. These data (*cf.* **TFRS-80ac**) showed no difference from cells fabricated using each of the pure samples, suggesting the retention of all device performances.

Fig. 3a exhibits the incident photon-to-current conversion efficiency (IPCE) action spectra recorded using I^-/I_3^- electrolyte I–A. The onset of the IPCE spectra of **TFRS-80a**, **80c**, and the mixture of **TFRS-80a** and **80c** are all close to ~780 nm, and with excellent IPCE performance in the range from 400 to 560 nm, among which the highest IPCE of 78% is recorded at around 530 nm, while **TFRS-80b** showed a notably lowered IPCE of only 51% at the same position. Apparently, the symmetrical **TFRS-80a** and **80c** exhibit much better IPCE action spectra as well as superior *J–V* characteristics, *versus* those exhibited by the asymmetric stereoisomer **80b**. It appears to us that the significantly reduced dye loading of **80b** on the TiO_2 surface, which not only reduced the absorptivity of **80b** on TiO_2 (Fig. 1) but also increased the charge recombination at the TiO_2/electrolyte interface, is the major contributing factor for the poor overall conversion efficiency detected.

Next, the photovoltaic performance of these sensitizers was evaluated by using $Co(phen)_3]^{2+/3+}$ based redox mediator in acetonitrile solution (*i.e.* Co-phen). A TiO_2 blocking layer was pre-deposited on FTO glass using an aqueous $TiCl_4$ solution. This measure is for retarding charge recombination between FTO and the $Co^{2+/3+}$ mediator in electrolyte.[25] Interestingly, the DSC device fabricated using **TFRS-80c** and $[Co(phen)_3]^{2+/3+}$ redox couple afforded the highest performance characteristics of J_{SC} = 14.32 mA cm^{-2}, V_{OC} = 840 mV, and FF = 0.754, corresponding to an overall η = 9.06% under AM 1.5G one sun irradiation. We attribute this to the diaxial arrangement of the isoquinolinyl substituents on the Ru(II) metal complex, on which the bulky 2,6-dialkoxyphenyl group is expected to form a closely packed insulation layer, as they are now lying directly on top of the TiO_2 electrode surface.[26] This spatial arrangement is expected to be very effective in preventing the oxidized Co^{3+} species from approaching close to the TiO_2 surface in comparison with the other isomers **80a** and **80b**, for which there is at least one 2,6-dialkoxyphenyl group per molecule orientated

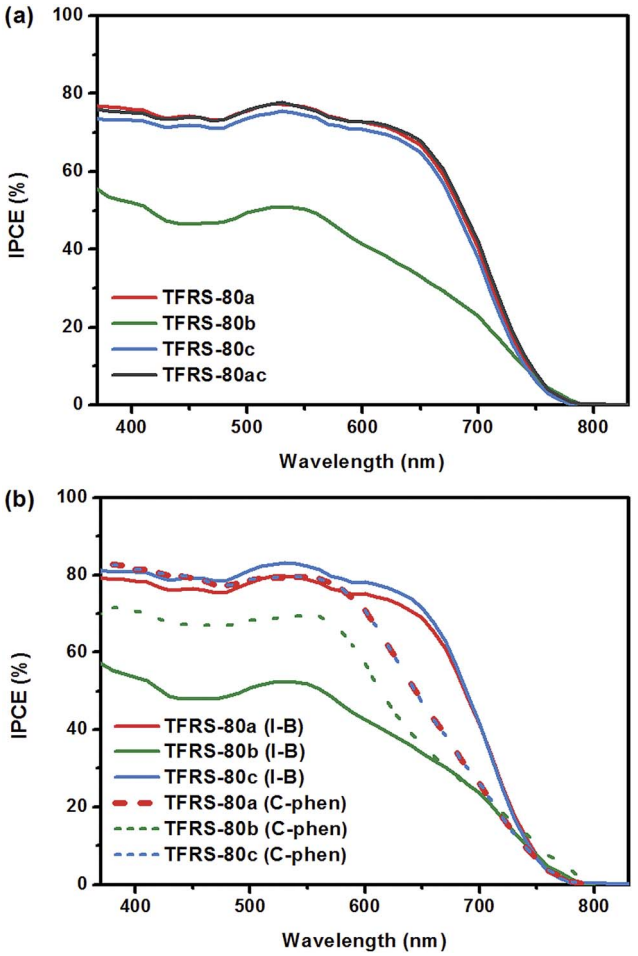

Fig. 3 IPCE action spectra for DSC cells fabricated using (a) electrolyte I–A and (b) electrolyte Co-phen and another I^-/I_3^- electrolyte I–B under AM1.5 solar irradiation.

further away from the TiO_2 surface, and cannot be effective in suppressing the charge recombination against the accumulated, oxidized Co^{3+} metal species.

For a further comparison, all sensitizers were subjected to DSC fabrication using the I^-/I_3^- reference electrolyte (*i.e.* electrolyte I–B) under identical cell parameters. As can be seen, the overall efficiencies span the range 4.80–7.55%, among which the best one is that fabricated using **TFRS-80a**. In comparison across the different electrolytes, these data remain 1.0% lower than those documented for the cell fabricated using the corresponding sensitizer and the $[Co(phen)_3]^{2+/3+}$ electrolyte Co-phen. For **TFRS-80c**, the difference increases to approx. 2.0%, which is even greater. Moreover, the DSC device fabricated using **TFRS-80b** and I^-/I_3^- electrolyte I–B showed the worst overall η of 4.80%. These data are much inferior to those observed for the $Co^{2+/3+}$ based cell, with performance data of J_{SC} = 13.30 mA cm^{-2}, V_{OC} = 820 mV, and FF = 0.766, corresponding to an overall η = 8.36%. The latter result is probably due to the effective insulating power of this sensitizer against the bulky Co^{3+} metal species, leading to the more effective suppression of charge recombination. In addition, the lowered

efficiencies of all I^-/I_3^- based DSCs can be traced to the inferior V_{OC}, mainly caused by the greater loss-in-potential for the I^-/I_3^- redox couple *versus* the $Co^{2+/3+}$ electrolyte.

Moreover, the cell efficiency of **TFRS-80b** is ~2.5% lower than those of the symmetric counterparts, *i.e.* **TFRS-80a** and **TFRS-80c**, upon using the I^-/I_3^- based electrolytes I–A and I–B. On the other hand, the **TFRS-80b** sensitizer showed a much smaller difference of 0.7% in efficiency upon switching to $Co^{2+/3+}$ electrolyte, compared with the best **TFRS-80c**. Since all of these sensitizers have essentially identical spectroscopic and electrochemical properties, this large variation can only be explained by the inferior dye-loading for **TFRS-80b** that generated a larger number of voids on the TiO_2 surface. Accordingly, the I_3^- ion is much smaller and can penetrate much deeper into the dye layer *versus* that of $Co^{2+/3+}$ electrolyte, giving much greater charge recombination and the greater difference in efficiencies.

Fig. 3b exhibits the incident photon-to-current conversion efficiency (IPCE) action spectra recorded using the electrolytes Co-phen and I–B. Integration of the IPCE spectra yields the calculated J_{SC} data which are in good agreement with the experimental values. It is also notable that the $Co^{2+/3+}$ electrolyte exhibited the higher photocurrent response from 370 to 440 nm *versus* that of the I^-/I_3^- electrolyte, which is ascribed to the lower molar absorption coefficients of the $Co^{2+/3+}$ complexes in the high energy region compared with the I^-/I_3^- redox couple. Concurrently, similar to other reported Ru(II) sensitizers, we also observed a degradation of the photocurrent response in the lower energy region when switching to the $Co^{2+/3+}$ electrolyte.[27] This phenomenon is probably due to the poor dye regeneration efficiencies caused by the diminishing of the overpotential for dye regeneration.

For a closer comparison, the best recorded efficiency of **TFRS-80** series obtained in this study (9.06%) is slightly higher than that of recently reported tris-heteroleptic Ru(II) sensitizers with 2′,6′-dimethoxy-2,3′-bipyridine cyclometalate ($\eta = 8.6\%$).[27a] In turn, both data are superior to the thiocyanate-free Ru(II) sensitizer with ppy-$(CF_3)_2$ cyclometalate ($\eta = 5.5\%$),[11a] and traditional thiocyanate-containing Ru(II) sensitizers, such as: **N719** ($\eta = 1.8\%$) and **Z907** ($\eta = 6.5\%$),[27c] **Z907** with co-grafting phosphonic acid ($\eta = 8.4\%$),[27b] and **C101** ($\eta = 3.6\%$) and **TT-230** ($\eta = 1.8\%$).[28] It is notable that the **TT-230** dye was even functionalized with the cyclopenta(2,1-*b*:3,4-*b*′)dithiophene moieties,[29] which were widely used in organic push–pull dyes for extending the optical response, retarding charge recombination and suppressing dark current, but is still unable to boost its performances. On the other hand, DSCs with $Co^{2+/3+}$ electrolytes are known to display higher solar cell efficiency, if the employed organic sensitizers were decorated with adequate bulky and electron donating appendages[30] and with rigidified skeletal structure,[31] to bring forth the anticipated enhancement in both J_{SC} and V_{OC}, by avoiding the aggregation and facilitating the photo-induced electron transfer process.

To gain further insight into the rates of interfacial recombination of electrons from the TiO_2 conduction band to the redox mediators in the electrolyte, variation of the TiO_2 conduction band potential was accessed by measuring the capacitance for three DSC devices at each V_{OC} using the charge extraction (CE) method and intensity-modulated photovoltage spectroscopy (IMVS) measurement. Comparing that of **TFRS-80a** and **80c**, a lower V_{OC} for **TFRS-80b** is noticed (see Table 3). As shown in Fig. 4a, the CE results indicate that the TiO_2 conduction band potential of the devices with the Co-phen

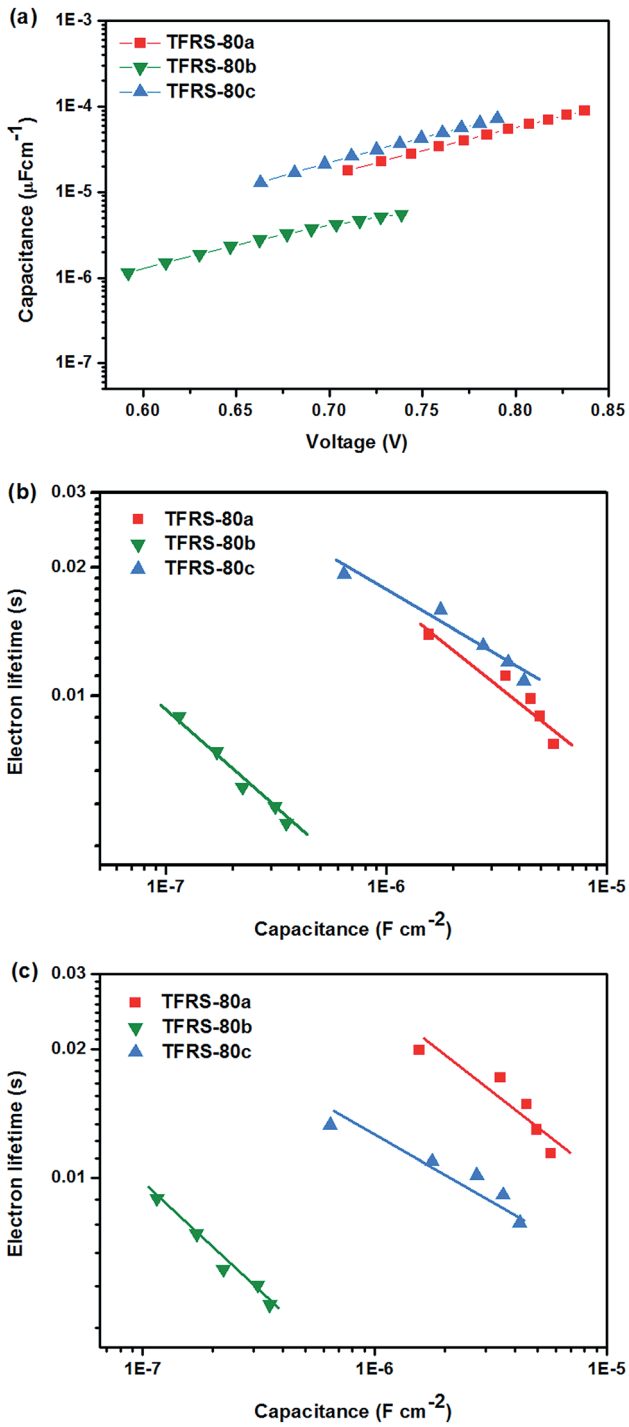

Fig. 4 (a) Electron density *versus* voltage deduced from charge extraction measurement; (b) IMVS measurement for cells using the electrolyte Co-phen and (c) IMVS measurement for cells using I^-/I_3^- electrolyte I–B.

electrolyte showed a systematic upward shift in the order **TFRS-80b** < **80c** < **80a**, consistent with the variation of their V_{OC}.[32] Fig. 4b and c show plots of electron lifetime under five different light intensities. The results indicate a systematic trend with the electron lifetime showing an order of **TFRS-80c** > **80a** > **80b** for the Co-phen electrolyte and the order of **TFRS-80a** > **80c** > **80b** for the electrolyte I–B, respectively. These trends correspond to the degree of charge recombination, and are also consistent with the variation of V_{OC} for these devices. Normally, the electron lifetime has the opposite trend *versus* charge recombination. Longer electron lifetime would correspond to smaller charge recombination loss and higher V_{OC} in solar cells. Additionally, the electron lifetime of **TFRS-80c** is the highest for all the cells using $Co^{2+/3+}$ based electrolyte. Thus, this proves the non-accumulation of Co^{3+} species in the proximity of TiO_2 surface and the decrease in charge recombination due to the efficient blocking effect of TFRS sensitizers.

Conclusion

To sum up, we have designed and prepared a series of thiocyanate-free Ru(II) sensitizers, *i.e.* **TFRS-80a**, **80b** and **80c**, all with similar electrochemical properties and identical optical response under simulated one sun illumination, but showing varied steric impediment upon depositing on TiO_2 surface according to the coordination orientation of the tpiq ancillaries. Among the photophysical and electrochemical parameters collected, the hole-diffusion coefficients are the most important, which follow the trend of **TFRS-80a** > **80b** > **80c** (4.21, 1.28 and 0.203×10^{-10} cm^2 s^{-1}). This trend supports the effective blockage of π–π interactions by 2,6-dihexyloxylphenyl substituents, since **TFRS-80a**, **80b** and **80c** have respectively zero, one and two tpiq arms in position to minimize dye–dye interactions on the TiO_2 surface.

DSCs with I^-/I_3^- electrolyte were first fabricated, among which the **TFRS-80a** and **TFRS-80b** showed the highest and the lowest efficiencies of $\eta = 8.37$ and 5.55%, for which the large variation was mainly determined by the amount of dye uptake and hence, give decreased light harvesting capability and enhanced charge recombination across the TiO_2-dye–electrolyte interface for the asymmetric **TFRS-80b**. In sharp contrast, DSCs with $[Co(phen)_3]^{2+/3+}$ electrolyte showed much superior efficiencies for all **TFRS-80** sensitizers and, most importantly, the detected efficiency increased to $\eta = 9.06\%$ in the symmetrical **TFRS-80a**. Their advantages are apparently due to the combination of several factors, namely: (i) charge neutrality, (ii) absence of thiocyanate ligands, (iii) enhanced dye loading, and (iv) adequate spatial impediment upon depositing on TiO_2 surface. All these contributing factors are essential for preventing the strong association to the $Co^{2+/3+}$ mediator, which therefore reduces the charge recombination across the interface of TiO_2 and electrolyte. The knowledge gained in this study should be of help to the future optimization of Ru(II) metal based sensitizers for DSC cells employing various $Co^{2+/3+}$ based mediators.

Experimental section

General procedures

All reactions were performed under nitrogen. Solvents were distilled from appropriate drying agents prior to use. Commercially available reagents were used without further purification. All reactions were monitored by TLC with precoated silica gel plates (Merck, 0.20 mm with fluorescent indicator UV254). Compounds were visualized with UV irradiation at 254 or 365 nm. Flash column chromatography was carried out using silica gel obtained from Merck (230–400 mesh). Mass spectra were obtained on a JEOL SX-102A instrument operating in electron impact (EI) or fast atom bombardment (FAB) mode. ^1H and ^{19}F NMR spectra were recorded on a Bruker-400 instrument. Photophysical data were obtained using an Edinburgh Fluorescence spectrometer FLS928P. Details of the synthetic protocols for the tri-dentate ancillary chelates and the procedures for the DFT calculations are all given in the ESI.†

Synthesis of TFRS-80a, 80b and 80c

A xylene solution of 6-(5-(2,6-bis(hexyloxy)phenyl)thiophen-2-yl)-1-(3-(trifluoromethyl)-1*H*-pyrazol-5-yl)isoquinoline (113 mg, 0.209 mmol), Ru(diethyl-2,2′-bipyridine-4,4′-dicarboxylate) (*p*-cymene)Cl (60 mg, 0.104 mmol), and KOAc (52 mg, 0.531 mmol) was heated at reflux under N_2 for 6 h. After the removal of solvent under vacuum, the residue was dissolved in CH_2Cl_2 and washed with water (3 × 20 mL). Concentration of this CH_2Cl_2 solution gave a dark-brown oily solid. It was then purified by silica gel column chromatography eluting with a 1 : 4 mixture of ethyl acetate and hexane to afford a mixture of isomers **a** and **c** and analytically pure isomer **b**. Then, analytically pure **a** and **c** were separated by a second silica gel column chromatography using a 1 : 20 mixture of ethyl acetate and CH_2Cl_2.

For hydrolysis, each of the samples was dissolved in a mixed acetone (20 mL) and 1 M NaOH solution (0.1 mL), and heated to reflux under N_2 for 3 h. After this, the solution was diluted with water (10 mL) and, then, acidified with 2 M HCl to pH 3 to afford a brown precipitate. This was collected and washed with water, acetone, and diethylether in sequence, yield: 52 mg, 32% for **TFRS-80a**, 18 mg, 11% for **TFRS-80b**, and 25 mg, 15% for **TFRS-80c**.

Spectral data of TFRS-80a. MS (FAB, ^{102}Ru): *m*/*z* 1588 $(M+1)^+$. ^1H NMR (400 MHz, d_6-DMSO, 298 K): δ 8.98 (s, 2H), 8.86 (d, J = 9.2 Hz, 2H), 8.14 (d, J = 6.0 Hz, 2H), 8.07 (s, 2H), 8.01 (d, J = 8.8 Hz, 2H), 7.83 (s, 2H), 7.74 (d, J = 6.0 Hz, 2H), 7.68 (d, J = 4.0 Hz, 2H), 7.57 (d, J = 4.0 Hz, 2H), 7.53 (d, J = 6.8 Hz, 2H), 7.21 (t, J = 8.4 Hz, 2H), 7.04 (d, J = 6.4 Hz, 2H), 6.70 (d, J = 8.4 Hz, 4H), 3.99 (t, J = 6.4 Hz, 8H), 1.71 (m, 8H), 1.38 (m, 8H), 1.22 (m, 16H), 0.74 (t, J = 6.8 Hz, 12H). ^{19}F NMR (376 MHz, d_6-DMSO, 298 K): δ −60.12 (s, 6F). Anal. calcd for $C_{82}H_{82}F_6N_8O_8RuS_2 \cdot H_2O$: C, 61.37; N, 6.98; H, 5.28%. Found: C, 61.21; N, 6.71; H, 5.44%.

Spectral data of TFRS-80b. MS (FAB, ^{102}Ru): *m*/*z* 1587 $(M)^+$. ^1H NMR (400 MHz, d_6-DMSO, 298 K): δ 8.90 (m, 4H), δ 8.18 (s, 1H), δ 8.13 (s, 1H), 8.07 (d, J = 8.0 Hz 2H), 8.01 (m, 1H), 7.83 (s, 1H), 7.77 (m, 5H), 7.71 (s, 1H), 7.61 (t, J = 3.6 Hz, 2H), 7.51 (d, J = 6.4 Hz, 1H), 7.45 (d, J = 6.4 Hz, 1H), 7.39 (d, J = 6.4 Hz, 1H),

7.33 (d, $J = 6.4$ Hz, 1H), 7.24 (m, 2H), 6.77 (d, $J = 3.6$ Hz, 2H), 6.75 (d, $J = 4.0$ Hz, 2H), 4.05 (m, 8H), 1.74 (m, 8H), 1.27 (m, 8H), 1.23 (m, 16H), 0.79 (t, $J = 6.8$ Hz, 12H). ^{19}F NMR (376 MHz, d_6-DMSO, 298 K): δ −57.74 (s, 3F), −57.79 (s, 3F). Anal. calcd for $C_{82}H_{82}F_6N_8O_8RuS_2 \cdot 2H_2O$: C, 60.69; N, 7.02; H, 5.34%. Found: C, 60.56; N, 6.74; H, 5.49%.

Spectral data of TFRS-80c. MS (FAB, ^{102}Ru): m/z 1587 $(M)^+$. ^{1}H NMR (400 MHz, d_6-DMSO, 298 K): δ 8.86 (d, $J = 4.4$ Hz, 2H), 8.76 (s, 2H), 8.06 (s, 2H), 8.02 (d, $J = 9.2$ Hz, 2H), 7.91 (d, $J = 5.2$ Hz, 2H), 7.80 (s, 2H), 7.69 (d, $J = 3.6$ Hz, 2H), 7.63 (d, $J = 5.6$ Hz, 2H), 7.58 (d, $J = 3.6$ Hz, 2H), 7.49 (d, $J = 6.4$ Hz, 2H), 7.22 (t, $J = 8.4$ Hz, 2H), 7.07 (d, $J = 6.4$ Hz, 2H), 6.72 (d, $J = 8.4$ Hz, 4H), 4.00 (t, $J = 6.0$ Hz, 8H), 1.71 (m, 8H), 1.39 (m, 8H), 1.22 (m, 16H), 0.75 (t, $J = 6.8$ Hz, 12H). ^{19}F NMR (376 MHz, d_6-DMSO, 298 K): δ −57.91 (s, 6F). Anal. calcd for $C_{82}H_{82}F_6N_8O_8RuS_2 \cdot H_2O$: C, 61.37; N, 6.98; H, 5.28%. Found: C, 61.33; N, 6.75; H, 5.34%.

Device fabrication

The cells consisted of a 3.6 μm transparent layer of 20 nm TiO_2 nanoparticles, on which was superimposed a second layer, 3.5 μm of 400 nm TiO_2 nanoparticles for enhancing light scattering. This double layer film was heated to 500 °C, sintered for 30 min, cooled to 80 °C, and then immersed into the dye solution (0.3 mM) containing 10 vol.% DMSO and 2 eq. of tetrabutylammonium deoxycholate [TBA][DOC] in anhydrous ethanol for 12 h. The iodine electrolyte I–A contains 0.6 M DMPII (1,2-dimethyl-3-propyl-imidazolium iodide), 0.05 M I_2, 0.5 M TBP (4-*tert*-butylpyridine) in acetonitrile. The cobalt electrolyte Co-phen contains 0.45 M $[Co(phen)_3][TFSI]_2$, 0.15 M $[Co(phen)_3][TFSI]_3$, 0.15 M LiTFSI, and 0.8 M TBP in acetonitrile. The iodine electrolyte I–B contains 0.45 M DMPII, 0.05 M I_2, 0.15 M LiI, and 0.8 M TBP in acetonitrile. The counter electrodes were coated with an ultra-thin layer of the PVP capped platinum nanoclusters (PVP–Pt) in aqueous solution *via* a so-called "two-step dip coating" process on FTO glass (7 Ω/TEC7, 2.2 mm thick, Pilkington), followed by a post heating at 325 °C for 10 min.[33] The dye sensitized TiO_2 electrodes were assembled with Pt counter electrodes by inserting a hot-melt Surlyn film (Meltonix 1170–25, 25 μm, Solaronix) as spacer, and then heated at 130 °C. The electrolyte was injected into the cell through a predrilled hole at the counter electrode. The hole was sealed with a Surlyn sheet and a thin glass to avoid leakage. All fabricated DSC cells consist of an active area of 5 × 5 mm^2, and the performances were measured using a black metal mask with an aperture area of 4 × 4 mm^2.

Electrochemical characterization of dyes on TiO_2

Conductive FTO glass slides were cleaned with soap, water, deionized water, acetone and ethanol, dried under hot air and TiO_2 paste (Dyesol 18 NR-T) was deposited on the FTO glass *via* doctor blading. The films were sintered at 450 °C for 30 min; the resulting film thicknesses were ~6 μm. After cooling, the films were left in the dye bath (0.3 mM in DMSO–EtOH (v/v, 1 : 9)) for 30 h, then rinsed in acetonitrile for 1 min. Cyclic voltammetry (CV) measurements were performed using a three-electrode cell with the FTO/dyed-TiO_2 film as the working electrode, a Pt rod counter electrode and an Ag/AgCl reference electrode. The electrolyte composition was 0.1 M $TBAPF_6$ dissolved in acetonitrile bubbled with nitrogen for 15 min before the experiment.

Photovoltaic characterization

Photovoltaic measurements were carried out under a class-AAA solar simulator (Model 11016A, Sun 3000, ABET Technologies) equipped with a 550 W xenon light source and water-cooling stage (25 °C). The output power density was calibrated to be 100 mW cm^{-2} using a certificated KG-5 Si reference cell and with a circular aperture of 8 mm. The current–voltage characteristic of each cell was obtained with a 4-wire sense mode, delay time set as 100 ms and bias scan from short-circuit to open-circuit by using a Keithley digital source meter (Model 2400). The spectra of the incident photon-to-current conversion efficiency (IPCE) were calculated with the equation $1240 J_{SC}(\lambda)/(\lambda \mathrm{Pin}(\lambda))$ where J_{SC} is the short-circuit current density under each monochromatic illumination in units of A cm^{-2}, λ is the wavelength of incident monochromatic light in units of nanometers, and Pin is the monochromatic light intensity in units of W cm^{-2}, plotted as a function of incident wavelength with an increment of 10 nm. The current was pre-amplified by a current amplifier (SR570) and measured by Keithley 2400 source meter. It should be noted that 10 sets of J_{SC} (interval 50 ms) were collected sequentially after illuminating the device for 3 seconds and then averaged for calculation of IPCE. A 300 W Xe lamp (Model 6258, Newport Oriel) combined with an Oriel cornerstone 260 1/4 m monochromator (Model 74100) provided a monochromatic beam (dc mode) for the device under test conditions. The beam power intensity was calibrated with a power meter (Model 1936-C, Newport) equipped with a Newport 818-UV photodetector.

Charge extraction and intensity-modulated photovoltage spectroscopy

Charge extraction was measured with the PGSTAT302N electrochemical workstation (Autolab) at open-circuit condition for the photovoltage of the device to attain a steady state. A red light-emitting diode (LED, 627 nm) was attenuated while the device simultaneously switched to a short-circuit condition to measure the excess charges generated in the film. Intensity-modulated photovoltage spectroscopy (IMVS) measurement was conducted using the same electrochemical workstation equipped with a frequency response analyzer (FRA) to drive the red LED. Photovoltage response of the cells was analyzed in the frequency range of 1–10^4 Hz and LED supplied the AC (modulation depth 10%) perturbation current superimposed on the DC current.

Acknowledgements

This research was supported by Ministry of Science and technology of Taiwan, MOST 100-2119-M-002-008, and the UK EPSRC Global Grant EP/K004468. YH thanks the China Scholarship Council and the University of Edinburgh for a studentship.

References

1 (*a*) L. M. Goncalves, V. de Zea Bermudez, H. A. Ribeiro and A. M. Mendes, *Energy Environ. Sci.*, 2008, **1**, 655; (*b*) A. Hagfeldt, G. Boschloo, L. Sun, L. Kloo and H. Pettersson, *Chem. Rev.*, 2010, **110**, 6595; (*c*) J.-H. Yum, E. Baranoff, S. Wenger, M. K. Nazeeruddin and M. Grätzel, *Energy Environ. Sci.*, 2011, **4**, 842; (*d*) Y. Bai, I. Mora-Seró, F. De Angelis, J. Bisquert and P. Wang, *Chem. Rev.*, 2014, **114**, 10095.

2 (*a*) S. Mathew, A. Yella, P. Gao, R. Humphry-Baker, F. E. CurchodBasile, N. Ashari-Astani, I. Tavernelli, U. Rothlisberger, M. K. Nazeeruddin and M. Grätzel, *Nat. Chem.*, 2014, **6**, 242; (*b*) A. Yella, C.-L. Mai, S. M. Zakeeruddin, S.-N. Chang, C.-H. Hsieh, C.-Y. Yeh and M. Grätzel, *Angew. Chem., Int. Ed.*, 2014, **53**, 2973.

3 (*a*) A. Mishra, M. K. R. Fischer and P. Bäuerle, *Angew. Chem., Int. Ed.*, 2009, **48**, 2474; (*b*) Z. Ning, Y. Fu and H. Tian, *Energy Environ. Sci.*, 2010, **3**, 1170; (*c*) Y. Wu and W. Zhu, *Chem. Soc. Rev.*, 2013, **42**, 2039; (*d*) Y.-S. Yen, H.-H. Chou, Y.-C. Chen, C.-Y. Hsu and J. T. Lin, *J. Mater. Chem.*, 2012, **22**, 8734; (*e*) Y. Ooyama and Y. Harima, *ChemPhysChem*, 2012, **13**, 4032; (*f*) S. Ito, H. Miura, S. Uchida, M. Takata, K. Sumioka, P. Liska, P. Comte, P. Pechy and M. Grätzel, *Chem. Commun.*, 2008, 5194; (*g*) G. Zhang, H. Bala, Y. Cheng, D. Shi, X. Lv, Q. Yu and P. Wang, *Chem. Commun.*, 2009, 2198; (*h*) Q. Yu, D. Zhou, Y. Shi, X. Si, Y. Wang and P. Wang, *Energy Environ. Sci.*, 2010, **3**, 1722; (*i*) J.-H. Yum, E. Baranoff, F. Kessler, T. Moehl, S. Ahmad, T. Bessho, A. Marchioro, E. Ghadiri, J.-E. Moser, C. Yi, M. K. Nazeeruddin and M. Grätzel, *Nat. Commun.*, 2012, **3**, 631.

4 C. Chen, X. Yang, M. Cheng, F. Zhang and L. Sun, *ChemSusChem*, 2013, **6**, 1270.

5 B. Zietz, E. Gabrielsson, V. Johansson, A. M. El-Zohry, L. Sun and L. Kloo, *Phys. Chem. Chem. Phys.*, 2014, **16**, 2251.

6 (*a*) M. Zhang, J. Zhang, Y. Fan, L. Yang, Y. Wang, R. Li and P. Wang, *Energy Environ. Sci*, 2013, **6**, 2939; (*b*) M. Zhang, Y. Wang, M. Xu, W. Ma, R. Li and P. Wang, *Energy Environ. Sci.*, 2013, **6**, 2944.

7 (*a*) M. K. Nazeeruddin, P. Péchy, T. Renouard, S. M. Zakeeruddin, R. Humphry-Baker, P. Comte, P. Liska, L. Cevey, E. Costa, V. Shklover, L. Spiccia, G. B. Deacon, C. A. Bignozzi and M. Grätzel, *J. Am. Chem. Soc.*, 2001, **123**, 1613; (*b*) J.-H. Yum, I. Jung, C. Baik, J. Ko, M. K. Nazeeruddin and M. Grätzel, *Energy Environ. Sci.*, 2009, **2**, 100; (*c*) Y. Cao, Y. Bai, Q. Yu, Y. Cheng, S. Liu, D. Shi, F. Gao and P. Wang, *J. Phys. Chem. C*, 2009, **113**, 6290; (*d*) L. H. Nguyen, H. K. Mulmudi, D. Sabba, S. A. Kulkarni, S. K. Batabyal, K. Nonomura, M. Grätzel and S. G. Mhaisalkar, *Phys. Chem. Chem. Phys.*, 2012, **14**, 16182; (*e*) S.-W. Wang, C.-C. Chou, F.-C. Hu, K.-L. Wu, Y. Chi, J. N. Clifford, E. J. Palomares, S.-H. Liun, P.-T. Chou, T. C. Wei and T. Y. Hsiao, *J. Mater. Chem. A*, 2014, **2**, 17618.

8 A. Hinsch, W. Veurman, H. Brandt, K. Flarup Jensen and S. Mastroianni , *ChemPhysChem*, 2014, **15**, 1076.

9 (*a*) S. H. Wadman, J. M. Kroon, K. Bakker, M. Lutz, A. L. Spek, G. P. M. van Klink and G. van Koten, *Chem. Commun.*, 2007, 1907; (*b*) S. H. Wadman, J. M. Kroon, K. Bakker, R. W. A. Havenith, G. P. M. van Klink and G. van Koten, *Organometallics*, 2010, **29**, 1569.

10 (*a*) T. Bessho, E. Yoneda, J.-H. Yum, M. Guglielmi, I. Tavernelli, H. Imai, U. Rothlisberger, M. K. Nazeeruddin and M. Grätzel, *J. Am. Chem. Soc.*, 2009, **131**, 5930; (*b*) F. De Angelis, S. Fantacci, A. Selloni, M. K. Nazeeruddin and M. Grätzel, *J. Phys. Chem. C*, 2010, **114**, 6054.

11 (*a*) P. G. Bomben, T. J. Gordon, E. Schott and C. P. Berlinguette, *Angew. Chem., Int. Ed.*, 2011, **50**, 10682; (*b*) P. G. Bomben, K. C. D. Robson, B. D. Koivisto and C. P. Berlinguette, *Coord. Chem. Rev.*, 2012, **256**, 1438; (*c*) K. C. D. Robson, P. G. Bomben and C. P. Berlinguette, *Dalton Trans.*, 2012, **41**, 7814; (*d*) S. Sinn, B. Schulze, C. Friebe, D. G. Brown, M. Jäger, E. Altuntaş, J. Kübel, O. Guntner, C. P. Berlinguette, B. Dietzek and U. S. Schubert, *Inorg. Chem.*, 2014, **53**, 2083.

12 (*a*) B.-S. Chen, K. Chen, Y.-H. Hong, W.-H. Liu, T.-H. Li, C.-H. Lai, P.-T. Chou, Y. Chi and G.-H. Lee, *Chem. Commun.*, 2009, 5844; (*b*) K.-L. Wu, H.-C. Hsu, K. Chen, Y. Chi, M.-W. Chung, W.-H. Liu and P.-T. Chou, *Chem. Commun.*, 2010, **46**, 5124; (*c*) Y. Chi, B. Tong and P.-T. Chou, *Coord. Chem. Rev.*, 2014, **281**, 1.

13 (*a*) C.-C. Chou, K.-L. Wu, Y. Chi, W.-P. Hu, S. J. Yu, G.-H. Lee, C.-L. Lin and P.-T. Chou, *Angew. Chem., Int. Ed.*, 2011, **50**, 2054; (*b*) K.-L. Wu, S.-T. Ho, C.-C. Chou, Y.-C. Chang, H.-A. Pan, Y. Chi and P.-T. Chou, *Angew. Chem., Int. Ed.*, 2012, **51**, 5642; (*c*) C.-C. Chou, F.-C. Hu, H.-H. Yeh, H.-P. Wu, Y. Chi, J. N. Clifford, E. Palomares, S.-H. Liu, P.-T. Chou and G.-H. Lee, *Angew. Chem., Int. Ed.*, 2014, **53**, 178.

14 (*a*) C.-W. Hsu, S.-T. Ho, K.-L. Wu, Y. Chi, S.-H. Liu and P.-T. Chou, *Energy Environ. Sci.*, 2012, **5**, 7549; (*b*) C.-C. Chou, P.-H. Chen, F.-C. Hu, Y. Chi, S.-T. Ho, J.-J. Kai, S.-H. Liu and P.-T. Chou, *J. Mater. Chem. A*, 2014, **2**, 5418.

15 (*a*) K.-L. Wu, W.-P. Ku, J. N. Clifford, E. Palomares, S.-T. Ho, Y. Chi, S.-H. Liu, P.-T. Chou, M. K. Nazeeruddin and M. Grätzel, *Energy Environ. Sci.*, 2013, **6**, 859; (*b*) S.-W. Wang, K.-L. Wu, E. Ghadiri, M. G. Lobello, S.-T. Ho, Y. Chi, J.-E. Moser, F. De Angelis, M. Grätzel and M. K. Nazeeruddin, *Chem. Sci.*, 2013, **4**, 2423.

16 K.-L. Wu, J. N. Clifford, S.-W. Wang, Y. Aswani, E. Palomares, M. G. Lobello, E. Mosconi, F. De Angelis, W.-P. Ku, Y. Chi, M. K. Nazeeruddin and M. Grätzel, *ChemSusChem*, 2014, **7**, 2930.

17 F.-C. Hu, S.-W. Wang, Y. Chi, N. Robertson, T. Hewat, Y. Hu, S.-H. Liu, P.-T. Chou, P.-F. Yang and H.-W. Lin, *ChemPhysChem*, 2014, **15**, 1207.

18 (*a*) C.-L. Wang, J.-Y. Hu, C.-H. Wu, H.-H. Kuo, Y.-C. Chang, Z.-J. Lan, H.-P. Wu, E. Wei-Guang Diau and C.-Y. Lin, *Energy Environ. Sci.*, 2014, **7**, 1392; (*b*) Z. Wang, H. Wang, M. Liang, Y. Tan, F. Cheng, Z. Sun and S. Xue, *ACS Appl. Mater. Interfaces*, 2014, **6**, 5768; (*c*) J. Yang, P. Ganesan, J. Teuscher, T. Moehl, Y. J. Kim, C. Yi, P. Comte, K. Pei, T. W. Holcombe, M. K. Nazeeruddin, J. Hua,

S. M. Zakeeruddin, H. Tian and M. Grätzel, *J. Am. Chem. Soc.*, 2014, **136**, 5722.

19 F. Gao, Y. Wang, D. Shi, J. Zhang, M. Wang, X. Jing, R. Humphry-Baker, P. Wang, S. M. Zakeeruddin and M. Grätzel, *J. Am. Chem. Soc.*, 2008, **130**, 10720.

20 F. Matar, T. H. Ghaddar, K. Walley, T. DosSantos, J. R. Durrant and B. O'Regan, *J. Mater. Chem.*, 2008, **18**, 4246.

21 (*a*) S.-Q. Fan, C. Kim, B. Fang, K.-X. Liao, G.-J. Yang, C.-J. Li, J.-J. Kim and J. Ko, *J. Phys. Chem. C*, 2011, **115**, 7747; (*b*) H. Ozawa, R. Shimizu and H. Arakawa, *RSC Adv.*, 2012, **2**, 3198; (*c*) L. Han, A. Islam, H. Chen, C. Malapaka, B. Chiranjeevi, S. Zhang, X. Yang and M. Yanagida, *Energy Environ. Sci.*, 2012, **5**, 6057.

22 (*a*) M. Liang and J. Chen, *Chem. Soc. Rev.*, 2013, **42**, 3453; (*b*) R. Stalder, D. Xie, A. Islam, L. Han, J. R. Reynolds and K. S. Schanze, *ACS Appl. Mater. Interfaces*, 2014, **6**, 8715.

23 (*a*) X. Li, M. K. Nazeeruddin, M. Thelakkat, P. R. F. Barnes, R. Vilar and J. R. Durrant, *Phys. Chem. Chem. Phys.*, 2011, **13**, 1575; (*b*) D. Moia, V. Vaissier, I. Lopez-Duarte, T. Torres, M. K. Nazeeruddin, B. C. O'Regan, J. Nelson and P. R. F. Barnes, *Chem. Sci.*, 2014, **5**, 281.

24 R. Jiang, A. Anderson, P. R. F. Barnes, L. Xiaoe, C. Law and B. C. O'Regan, *J. Mater. Chem. A*, 2014, **2**, 4751.

25 J.-H. Yum, T. Moehl, J. Yoon, A. K. Chandiran, F. Kessler, P. Gratia and M. Grätzel, *J. Phys. Chem. C*, 2014, **118**, 16799.

26 (*a*) S. Archer and J. A. Weinstein, *Coord. Chem. Rev.*, 2012, **256**, 2530; (*b*) L.-L. Li and E. W.-G. Diau, *Chem. Soc. Rev.*, 2013, **42**, 291.

27 (*a*) L. E. Polander, A. Yella, B. F. E. Curchod, A. N. Ashari, J. Teuscher, R. Scopelliti, P. Gao, S. Mathew, J.-E. Moser, I. Tavernelli, U. Rothlisberger, M. Gratzel, M. K. Nazeeruddin and J. Frey, *Angew. Chem., Int. Ed.*, 2013, **52**, 8731; (*b*) Y. Liu, J. R. Jennings, X. Wang and Q. Wang, *Phys. Chem. Chem. Phys.*, 2013, **15**, 6170; (*c*) Y. Liu, J. R. Jennings, Y. Huang, Q. Wang, S. M. Zakeeruddin and M. Grätzel, *J. Phys. Chem. C*, 2011, **115**, 18847.

28 S. A. Kumar, M. Urbani, M. Medel, M. Ince, D. González-Rodríguez, A. K. Chandiran, A. N. Bhaskarwar, T. Torres, M. K. Nazeeruddin and M. Grätzel, *J. Phys. Chem. Lett.*, 2014, **5**, 501.

29 (*a*) Q. Feng, X. Jia, G. Zhou and Z.-S. Wang, *Chem. Commun.*, 2013, **49**, 7445; (*b*) H. Ellis, S. K. Eriksson, S. M. Feldt, E. Gabrielsson, P. W. Lohse, R. Lindblad, L. Sun, H. Rensmo, G. Boschloo and A. Hagfeldt, *J. Phys. Chem. C*, 2013, **117**, 21029; (*c*) L. Cabau, L. Pelleja, J. N. Clifford, C. V. Kumar and E. Palomares, *J. Mater. Chem. A*, 2013, **1**, 8994.

30 M. Xu, M. Zhang, M. Pastore, R. Li, F. De Angelis and P. Wang, *Chem. Sci.*, 2012, **3**, 976.

31 N. Cai, J. Zhang, M. Xu, M. Zhang and P. Wang, *Adv. Funct. Mater.*, 2013, **23**, 3539.

32 T. Moehl, H. N. Tsao, K.-L. Wu, H.-C. Hsu, Y. Chi, E. Ronca, F. De Angelis, M. K. Nazeeruddin and M. Grätzel, *Chem. Mater.*, 2013, **25**, 4497.

33 T. C. Wei, C. C. Wan and Y. Y. Wang, *Appl. Phys. Lett.*, 2006, **88**, 103122.